

Azimuthal anisotropy: transition from hydrodynamic flow to jet suppression

Roy A. Lacey,^{1,2,*} A. Taranenko,¹ R. Wei,¹ N. N. Ajitanand,¹ J. M. Alexander,¹ J. Jia,^{1,2}
R. Pak,² Dirk H. Rischke,^{3,4} D. Teaney,^{5,2} and K. Dusling²

¹*Department of Chemistry, Stony Brook University,
Stony Brook, NY, 11794-3400, USA*

²*Physics Department, Brookhaven National Laboratory,
Upton, New York 11973-5000, USA*

³*Frankfurt Institute for Advanced Studies (FIAS), Frankfurt am Main, Germany*

⁴*Institut für Theoretische Physik, Johann Wolfgang Goethe-Universität
D-60438 Frankfurt am Main, Germany*

⁵*Department of Physics, Stony Brook University,
Stony Brook, NY, 11794-3800, USA*

(Dated: July 15, 2021)

Measured 2nd and 4th azimuthal anisotropy coefficients $v_{2,4}(N_{\text{part}}, p_T)$ are scaled with the initial eccentricity $\varepsilon_{2,4}(N_{\text{part}})$ of the collision zone and studied as a function of the number of participants N_{part} and the transverse momenta p_T . Scaling violations are observed for $p_T \lesssim 3$ GeV/c, consistent with a p_T^2 dependence of viscous corrections and a linear increase of the relaxation time with p_T . These empirical viscous corrections to flow and the thermal distribution function at freeze-out constrain estimates of the specific viscosity and the freeze-out temperature for two different models for the initial collision geometry. The apparent viscous corrections exhibit a sharp maximum for $p_T \gtrsim 3$ GeV/c, suggesting a breakdown of the hydrodynamic ansatz and the onset of a change from flow-driven to suppression-driven anisotropy.

PACS numbers: 25.75.Dw, 25.75.Ld

A central objective of the experimental program at the Relativistic Heavy Ion Collider (RHIC) is to delineate the thermodynamic and transport properties of the hot and dense matter produced in energetic heavy ion collisions. This matter can equilibrate to form a hot plasma of quarks and gluons (QGP)[1] which rapidly expands, cools, and then hadronize to produce the observed particles. The hydrodynamic-like expansion of the QGP, as well as its interactions with hard scattered partons, results in the anisotropic emission of hadrons relative to the reaction plane. At mid-rapidity, the magnitude of this momentum anisotropy is characterized by the even-order Fourier coefficients; $v_n = \langle e^{in(\Delta\phi)} \rangle$, $n = 2, 4, \dots$, where $\Delta\phi$ is the azimuth of an emitted hadron about the reaction plane, and brackets denote averaging over particles and events.

The coefficients for hadrons with low transverse momenta ($p_T \lesssim 2$ GeV/c) can be understood in terms of flow or partonic interactions which drive pressure gradients in an initial “almond-shaped” collision zone produced in non-central collisions [2–5]. For higher transverse momenta ($p_T \gtrsim 5$ GeV/c) the coefficients can be attributed to jet quenching [6] – the process by which hard scattered partons interact and lose energy in the hot and dense QGP, prior to fragmenting into hadrons. This energy loss manifests as a suppression of hadron yields [7] which depends on the average distance that partons propagate through the QGP. Thus, $v_{2,4}$ stem from the fact that partons which traverse the QGP medium in a direction parallel (perpendicular) to the reaction plane result in less (more) suppression due to shorter (longer)

parton propagation lengths [8–10]. This path-length dependence is exemplified in the recently observed scaling patterns for hadron suppression [11, 12]. The transition from flow-driven to suppression-driven anisotropy is still poorly understood, and it remains a challenge to find a single consistent theoretical framework that gives an explanation of $v_{2,4}$ measurements over the full p_T range.

The magnitude of $v_{2,4}$, as well as their detailed dependence on p_T and collision centrality (or number of participants N_{part}), give invaluable insights on the thermodynamic and transport coefficients of the QGP. In particular, flow measurements ($v_2(p_T)$ and $v_2(N_{\text{part}})$) have been used to estimate the specific shear viscosity (*i.e.*, the ratio of shear viscosity η to entropy density s of the plasma) via comparisons to viscous relativistic hydrodynamic calculations [13–17]. The reliability of these $\frac{\eta}{s}$ estimates is influenced not only by the uncertainties in the initial conditions for hydrodynamic evolution, but also by ambiguities in the departure from equilibrium on the freeze-out surface. For a viscous fluid, this distribution (f) is of the form

$$\frac{dN}{dy p_T dp_T d\phi} \sim f_0 + \delta f \equiv f_0 \left(1 + C \left(\frac{p_T}{T_f} \right)^{2-\alpha} \right), \quad (1)$$

where f_0 is the equilibrium distribution, T_f is the freeze-out temperature, $C \approx \frac{\eta}{3\tau s T_f}$ and α ranges between 0 and 1 [18, 19]; τ is the time scale of the expansion. The factor δf , which results from a finite shear viscosity, is known to dominate the calculated viscous corrections to $v_2(p_T)$ for $p_T \gtrsim 1$ GeV/c [19]. However, its momentum dependence

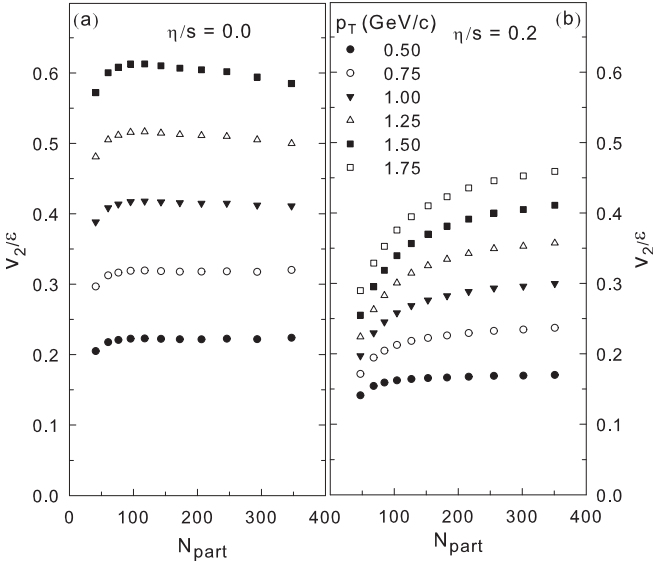


FIG. 1. (color online) Comparison of v_2/ε_2 vs. N_{part} for several p_T selections, obtained from perfect fluid (a) and viscous hydrodynamic (b) simulations [19] of Au+Au collisions.

and associated relaxation time $\tau_R(p)$ is not known *a priori*, and it is unclear whether or not it is proportional to p_T^2 ($\alpha = 0$ and $\tau_R \propto p$) as has been generally assumed in hydrodynamic calculations [13–17, 19]. The freeze-out temperature and the p_T for which large viscous corrections render a breakdown of viscous hydrodynamics are also not well established experimentally.

The influence of viscous corrections on the eccentricity-scaled anisotropy coefficient $\frac{v_2(N_{\text{part}}, p_T)}{\varepsilon_2(N_{\text{part}})}$ is illustrated in Figs. 1 (a) and (b) where the results of hydrodynamic simulations (with the code of Dusling and Teaney [19]) are shown for $\frac{\eta}{s} = 0$ and 0.2, respectively. Fig. 1 (b) shows that viscous effects reduce $v_2(N_{\text{part}}, p_T)$ and break the scale invariance of ideal hydrodynamics evidenced in Fig. 1 (a), *i.e.* there are deviations away from the essentially flat N_{part} dependence expected for ideal hydrodynamic scaling. These deviations from eccentricity-scaling can be used to estimate and characterize viscous corrections [19–23].

Here, we use the eccentricity scaled anisotropy coefficients, $\frac{v_2(N_{\text{part}}, p_T)}{\varepsilon_2(N_{\text{part}})}$ and $\frac{v_4(N_{\text{part}}, p_T)}{\varepsilon_4(N_{\text{part}})}$, to extract estimates of the viscous corrections to $v_{2,4}(p_T, N_{\text{part}})$. In turn, we use these estimates to explore the p_T dependence of δf and the transition from flow-driven to suppression-driven anisotropy. We find viscous correction factors for $p_T \lesssim 3$ GeV/c that validate the commonly assumed p_T^2 dependence of δf , and give constrained estimates for $\frac{\eta}{s}$ and the freeze-out temperature T_f . For $p_T \gtrsim 3$ GeV/c, the apparent viscous corrections signal a breakdown of the hydrodynamic ansatz.

The $v_{2,4}$ data employed in our analysis are selected from the high-precision PHENIX measurements recently

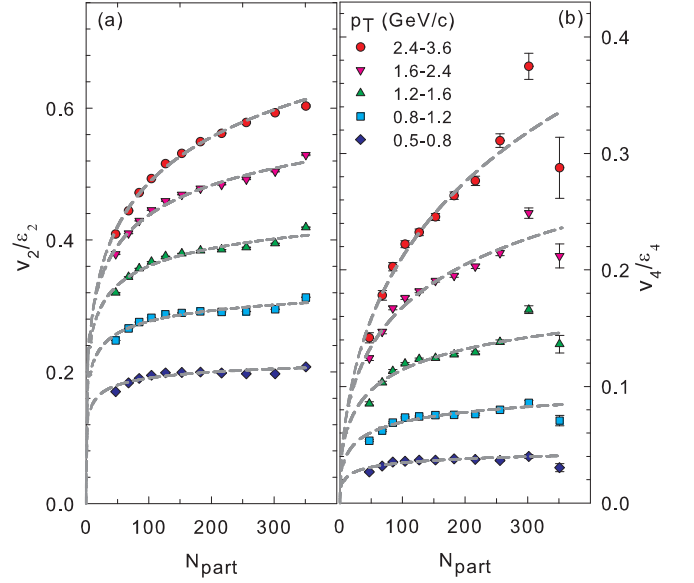


FIG. 2. (color online) Comparison of v_2/ε_2 vs. N_{part} (a) and v_4/ε_4 vs. N_{part} (b) for several p_T selections as indicated [24]. The dashed curves indicate a simultaneous fit to the data in (a) and (b) [for each p_T] with Eq. (3). The $v_{2,4}$ data are from Ref. [24].

reported for Au+Au collisions at $\sqrt{s_{NN}} = 200$ GeV [24]. These data show that both v_2 and v_4 have a strong dependence on p_T and centrality. The large increase in $v_{2,4}(p_T)$ from central to peripheral events is especially important to our study of viscous corrections.

Monte Carlo (MC) simulations [25] were used to calculate the event-averaged geometric quantities used in our analysis. For each collision, the values for N_{part} and the number of binary collisions N_{coll} were determined via the Glauber ansatz [26]. The associated values for the transverse size \bar{R} , area S and eccentricities $\varepsilon_{2,4}$ were then evaluated from the two-dimensional density of sources in the transverse plane $\rho_s(\mathbf{r}_\perp)$ using two principal models; a modified version of the MC-Glauber approach [26] and the factorized Kharzeev-Levin-Nardi (MC-KLN) model [27, 28].

For each event, we compute an event-shape vector S_n and the azimuth of rotation Ψ_n^* for the n -th harmonic of the shape profile [25];

$$S_{nx} \equiv S_n \cos(n\Psi_n^*) = \int d\mathbf{r}_\perp \rho_s(\mathbf{r}_\perp) \omega(\mathbf{r}_\perp) \cos(n\phi),$$

$$S_{ny} \equiv S_n \sin(n\Psi_n^*) = \int d\mathbf{r}_\perp \rho_s(\mathbf{r}_\perp) \omega(\mathbf{r}_\perp) \sin(n\phi),$$

$$\Psi_n^* = \frac{1}{n} \tan^{-1} \left(\frac{S_{ny}}{S_{nx}} \right),$$

where ϕ is the azimuthal angle of each source and the weight $\omega(\mathbf{r}_\perp) = \mathbf{r}_\perp^2$; $\varepsilon_{2,4}$ were calculated as:

$$\varepsilon_2 = \langle \cos 2(\phi - \Psi_2^*) \rangle, \quad \varepsilon_4 = \langle \cos 4(\phi - \Psi_2^*) \rangle, \quad (2)$$

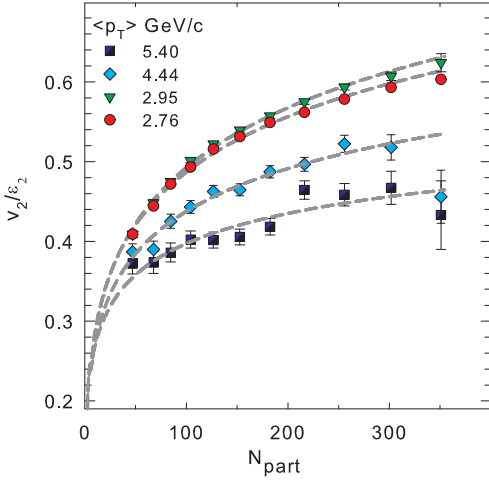


FIG. 3. (color online) v_2/ε_2 vs. N_{part} for several $\langle p_T \rangle$ values as indicated. The filled circles are the same as in Fig. 2(a). The dashed curves show fits to the data obtained with Eq. (3). The v_2 data are from Ref. [24].

127 where the brackets denote averaging over sources, as well
 128 as events belonging to a particular centrality or impact
 129 parameter range. For the MC-Glauber calculations, an
 130 additional entropy-density weight was applied reflecting
 131 the combination of spatial coordinates of participating
 132 nucleons and binary collisions [29];

$$\rho_s(\mathbf{r}_\perp) \propto \left[\frac{(1 - \alpha_1)}{2} \frac{dN_{\text{part}}}{d^2\mathbf{r}_\perp} + \alpha_1 \frac{dN_{\text{coll}}}{d^2\mathbf{r}_\perp} \right],$$

133 where $\alpha_1 = 0.14$ was constrained by multiplicity mea-
 134 surements as a function of N_{part} for Au+Au collisions
 135 [30]. Note that $\varepsilon_{2,4}$ (cf. Eq. (2)) correspond to $v_{2,4}$ mea-
 136 surements in the so-called participant plane [31]; this is
 137 analogous to the measurement of $v_{2,4}$ with respect to the
 138 2nd order event-plane as described in Ref. [24]. A corre-
 139 lation between the principal axes of the quadrupole (Ψ_2^*)
 140 and hexadecapole (Ψ_4^*) density profiles was also intro-
 141 duced to account for contributions to v_4 from v_2 [25].
 142 This correlation has a significant influence only on ε_4 in
 143 the most central collisions [25].

144 Figures 2 and 3 show eccentricity-scaled values of
 145 $v_{2,4}(p_T, N_{\text{part}})$ obtained with MC-KLN eccentricities for
 146 several p_T cuts. The low- p_T selections are almost flat,
 147 *i.e.* small scaling violations. These violations gradu-
 148 ally increase with p_T over the p_T range indicated in Fig.
 149 2. That is, the data points slope upward progressively
 150 (from low to high N_{part}) as the $\langle p_T \rangle$ is increased. Fig.
 151 3 shows that this trend reverses to give scaling viola-
 152 tions which decrease with increasing $\langle p_T \rangle$, for $\langle p_T \rangle \gtrsim 3$
 153 GeV/c. This inversion could be an indication for the on-
 154 set of suppression-driven anisotropy as discussed below.
 155 Similar scaling performed with MC-Glauber eccentrici-
 156 ties, show the same trends exhibited in Figs. 2 and 3,
 157 albeit with larger scaling violations, as discussed below.

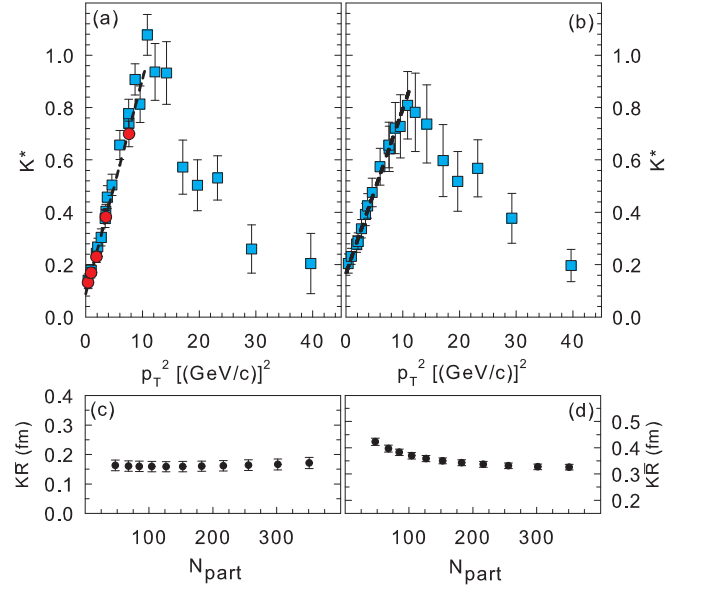


FIG. 4. (color online) K^* vs. $\langle p_T \rangle^2$ (a) and (b), and $K\bar{R}$ vs. N_{part} (c) and (d), extracted with MC-KLN (left panels) and MC-Glauber geometry (right panels). The filled circles in (a) indicate results from the simultaneous fits shown in Fig. 2. The dashed curves in (a) and (b) show a fit to the data for $\langle p_T \rangle^2 \lesssim 10$ [GeV/c]².

158 In lieu of detailed model comparisons [32], we estimate
 159 the magnitude of the viscous corrections by parametriz-
 160 ing the observed scaling violations with a Knudsen num-
 161 ber ($K = \lambda/\bar{R}$) ansatz akin to that in Refs. [20, 21];

$$\frac{v_{2k}(p_T)}{\varepsilon_{2k}} = \frac{v_{2k}^h(p_T)}{\varepsilon_{2k}} \left[\frac{1}{1 + \frac{K^*(p_T)}{K_0}} \right]^k \quad k = 1, 2, \dots, \quad (3)$$

162 where $K^*(p_T)$ characterizes the magnitude of the viscous
 163 correction for a given p_T , $\frac{v_{2,4}^h(p_T)}{\varepsilon_{2,4}}$ are the eccentricity-
 164 scaled coefficients expected from ideal hydrodynamics, λ
 165 is the mean-free path, and K_0 is a constant estimated to
 166 be 0.7 ± 0.03 with the aid of a transport model [33].

167 For each p_T selection, $[K^*(p_T)]^{-1} = \beta(p_T) \frac{1}{S} \frac{dN}{dy}$;
 168 $\left(\frac{dN}{dy} \propto N_{\text{part}}\right)$ is evaluated by fitting $\frac{v_{2,4}(p_T, N_{\text{part}})}{\varepsilon_{2,4}(N_{\text{part}})}$ vs.
 169 N_{part} with Eq. (3) (cf. curves in Figs 2 and 3). The
 170 fit parameters $\beta(p_T)$, so obtained, allow the determina-
 171 tion of $K^*(p_T)$ as a function of N_{part} . Note that a model
 172 uncertainty in the value of K_0 would lead to an accompa-
 173 nying uncertainty in the magnitude of K^* . However, the
 174 consistency of our procedure with hydrodynamic models
 175 has been tested via fits to $\frac{v_2(p_T, N_{\text{part}})}{\varepsilon_2(N_{\text{part}})}$ vs. N_{part} , obtained
 176 for specified values of $\frac{q}{s}$ [23]. These fits lead to $\frac{q}{s}$ values
 177 which reproduce the input values to the hydrodynamic
 178 simulations.

179 Figures 4 (a) and (b) show the values of K^* vs. p_T^2 , ex-
 180 tracted for $N_{\text{part}} \sim 351$ with MC-KLN and MC-Glauber
 181 geometries respectively (the plots for other values of

182 N_{part} show similar trends, but with different intercepts).
 183 The filled circles in Fig. 4 (a) show results from the simul-
 184 taneous fits indicated by the dashed curves in Figs. 2 (a)
 185 and (b). The squares show results for fits which employ
 186 only $\frac{v_2(p_T, N_{\text{part}})}{\varepsilon_2(N_{\text{part}})}$ data [24]; both are in good agreement.

187 The K^* values shown in Figs. 4 (a) and (b) indicate a
 188 linear dependence on p_T^2 , for $\langle p_T \rangle^2 \lesssim 10$ [GeV/c]², that
 189 demonstrates a non-zero viscosity and the p_T^2 dependence
 190 of δf commonly assumed in hydrodynamic simulations
 191 [13–17, 19]. In contrast, the data for $10 \lesssim \langle p_T \rangle^2 \lesssim 40$
 192 [GeV/c]² show a striking trend inversion. We interpret
 193 this as a signal for the breakdown of the hydrodynamic
 194 ansatz when $K^* \sim 1$, as well as an indication for the
 195 onset of suppression-driven anisotropy. Note that such
 196 a scenario would lead to improved eccentricity scaling
 197 for $p_T \gtrsim 3$ GeV/c because the eccentricity encodes the
 198 variation of the path length relative to the orientation of
 199 the reaction plane, and the suppression of hadron yields
 200 has been found to increase as $\frac{1}{\sqrt{p_T}}$ for a similar p_T range
 201 [12].

202 To obtain estimates for K and T_f for each value of
 203 N_{part} , we use our observation that $K^*(p_T) \propto p_T^2$ in
 204 conjunction with the first order expansion of $v_2(p_T) =$

$$205 \langle \cos(2\Delta\phi) \rangle_{p_T} \equiv \frac{\int_{-\pi}^{\pi} d\Delta\phi \cos(2\Delta\phi) \frac{d^3N}{dy p_t dp_t d\Delta\phi}}{\int_{-\pi}^{\pi} d\Delta\phi \frac{d^3N}{dy p_t dp_t d\Delta\phi}}, \text{ to obtain}$$

206 the expression $K^*(p_T) = K + \frac{B}{T_f} \left(\frac{p_T}{T_f} \right)^2$; the constant
 207 B was cross-checked via fits to the results from hydro-
 208 dynamic simulations. Fits to K^* vs. p_T^2 were performed
 209 with this fit function. The dashed curve in Fig. 4(a) indi-
 210 cates such a fit for $\langle p_T \rangle^2 \lesssim 10$ [GeV/c]²; it gives the val-
 211 ues $K = 0.09 \pm 0.01$ (from the intercept) and $T_f = 162 \pm 11$
 212 MeV (from the slope). The same fit to the K^* values in
 213 Fig. 4(b) (extracted with MC-Glauber eccentricities),
 214 give the values $K = 0.17 \pm 0.007$ and $T_f = 173 \pm 11$
 215 MeV. These same values of T_f are indicated by the fits
 216 to the data for other N_{part} values, for both data sets.
 217 However, as to be expected, the extracted K values vary
 218 with N_{part} . Note again that a model uncertainty in the
 219 value of K_0 would lead to an accompanying uncertainty
 220 in the magnitude of K and the associated values for λ
 221 and $\frac{\eta}{s}$ discussed below. The estimates for T_f are similar
 222 to the chemical freeze-out temperature ($T_c \sim 165$ MeV)
 223 obtained for a broad range of collision energies [34].

224 Figures 4 (c) and (d) show the product $K\bar{R}$ vs. N_{part} ,
 225 obtained with MC-KLN and MC-Glauber geometry res-
 226 spectively. Fig. 4 (c) indicates that the estimated value
 227 $\lambda \sim 0.17 \pm 0.018$ fm is essentially independent of N_{part} .
 228 Fig. 4 (d) indicates a larger estimate for central colli-
 229 sions $\lambda \sim 0.33 \pm 0.02$ fm, and a mild increase as collisions
 230 become more peripheral. While our analysis seems more
 231 consistent for the MC-KLN geometry, the model depen-
 232 dencies apparent in Fig. 4, highlight the importance of
 233 experimental signatures that can distinguish MC-KLN
 234 and MC-Glauber collision geometries [25].

235 Estimates for $\frac{\eta}{s}$ were obtained via the expression
 236 $\frac{\eta}{s} \approx \lambda T c_s \equiv (\bar{R} K T c_s)$ where the sound speed $c_s =$
 237 0.47 ± 0.03 c was obtained from lattice calculations [35] for
 238 the mean temperature $T = 220 \pm 20$ MeV [36]. This gives
 239 the estimates $4\pi\frac{\eta}{s} = 1.1 \pm 0.1$ and $4\pi\frac{\eta}{s} = 2.1 \pm 0.2$ for
 240 the K values extracted using MC-KLN and MC-Glauber col-
 241 lision eccentricities [respectively] in central and mid-central col-
 242 lisions. These estimates are in agreement with the low
 243 value from prior extractions [13–17, 19, 21, 23, 37–39].

244 In summary, we have used eccentricity scaled
 245 anisotropy coefficients to extract estimates of the
 246 strength and role of the viscous corrections. These es-
 247 timates show a quadratic increase with p_T (for $p_T \lesssim 3$
 248 GeV/c) that validates a non-zero viscosity and a relax-
 249 ation time which grows with p_T . The extracted vis-
 250 cous corrections also constrain the estimates $4\pi\frac{\eta}{s} \sim$
 251 1.1 ± 0.1 (2.1 ± 0.2) and $T_f = 162 \pm 11$ MeV (173 ± 11 MeV)
 252 for MC-KLN (MC-Glauber) collision geometries for a
 253 strongly coupled plasma. The onset of a transition from
 254 flow-driven to suppression-driven anisotropy is signaled
 255 by a sharp maximum of the apparent viscous corrections
 256 for $p_T \gtrsim 3$ GeV/c. These results provide valuable con-
 257 straints for input parameters to more detailed viscous
 258 hydrodynamic calculations.

259 **Acknowledgments** This research is supported by the
 260 US DOE under contract DE-FG02-87ER40331.A008 and
 261 by the NSF under award number PHY-0701487.

* E-mail: Roy.Lacey@Stonybrook.edu

- 262 [1] E. V. Shuryak, Phys. Lett., **B78**, 150 (1978).
 263 [2] J.-Y. Ollitrault, Phys. Rev., **D46**, 229 (1992).
 264 [3] U. Heinz and P. Kolb, Nucl. Phys., **A702**, 269 (2002).
 265 [4] E. Shuryak, Prog. Part. Nucl. Phys., **62**, 48 (2009).
 266 [5] R. Peschanski and E. N. Saridakis, Phys. Rev., **C80**,
 267 024907 (2009).
 268 [6] M. Gyulassy and X.-n. Wang, Nucl. Phys., **B420**, 583
 269 (1994).
 270 [7] K. Adcox *et al.*, Phys. Rev. Lett., **88**, 022301 (2002).
 271 [8] M. Gyulassy, I. Vitev, and X. N. Wang, Phys. Rev. Lett.,
 272 **86**, 2537 (2001).
 273 [9] X.-N. Wang, Phys. Rev., **C63**, 054902 (2001).
 274 [10] J. Liao and E. Shuryak, Phys. Rev. Lett., **102**, 202302
 275 (2009).
 276 [11] R. A. Lacey *et al.*, Phys. Rev., **C80**, 051901 (2009).
 277 [12] R. A. Lacey *et al.*, Phys. Rev. Lett., **103**, 142302 (2009).
 278 [13] P. Romatschke and U. Romatschke, Phys. Rev. Lett., **99**,
 279 172301 (2007).
 280 [14] M. Luzum and P. Romatschke, Phys. Rev., **C78**, 034915
 281 (2008).
 282 [15] H. Song and U. W. Heinz, J. Phys., **G36**, 064033 (2009).
 283 [16] A. K. Chaudhuri, (2009), [arXiv:0910.0979](https://arxiv.org/abs/0910.0979) [nucl-th].
 284 [17] G. S. Denicol, T. Kodama, and T. Koide, (2010),
 285 [arXiv:1002.2394](https://arxiv.org/abs/1002.2394) [nucl-th].
 286 [18] D. Teaney, Phys. Rev., **C68**, 034913 (2003).
 287 [19] K. Dusling, G. D. Moore, and D. Teaney, (2009),
 288 [arXiv:0909.0754](https://arxiv.org/abs/0909.0754) [nucl-th].
 289 [20] R. S. Bhalerao *et al.*, Phys. Lett., **B627**, 49 (2005).

- 291 [21] H.-J. Drescher, A. Dumitru, C. Gombeaud, and J.-Y. 307
292 Ollitrault, Phys. Rev., **C76**, 024905 (2007). 308
- 293 [22] H. Song and U. W. Heinz, Phys. Rev., **C78**, 024902 309
294 (2008), [arXiv:0805.1756 \[nucl-th\]](#). 310
- 295 [23] R. A. Lacey, A. Taranenko, and R. Wei, (2009), 311
296 [arXiv:0905.4368 \[nucl-ex\]](#). 312
- 297 [24] A. Adare *et al.*, (2010), [arXiv:1003.5586 \[nucl-ex\]](#). 313
- 298 [25] R. A. Lacey *et al.*, (2010), [arXiv:1002.0649 \[nucl-ex\]](#). 314
- 299 [26] M. L. Miller, K. Reygers, S. J. Sanders, and P. Steinberg, 315
300 Ann. Rev. Nucl. Part. Sci., **57**, 205 (2007). 316
- 301 [27] T. Lappi and R. Venugopalan, Phys. Rev., **C74**, 054905 317
302 (2006). 318
- 303 [28] H.-J. Drescher and Y. Nara, Phys. Rev., **C76**, 041903 319
304 (2007). 320
- 305 [29] T. Hirano and Y. Nara, Phys. Rev., **C79**, 064904 (2009).
306 [30] B. B. Back *et al.*, Phys. Rev., **C70**, 021902 (2004). 320
- [31] B. Alver *et al.*, Phys. Rev. Lett., **98**, 242302 (2007).
[32] Such comparisons are in progress and will be presented elsewhere.
[33] C. Gombeaud and J. Y. Ollitrault, Phys. Rev. C77, 054904, 2008.
[34] J. Cleymans, H. Oeschler, K. Redlich, and S. Wheaton, Phys. Rev., **C73**, 034905 (2006).
[35] P. Huovinen and P. Petreczky, Nucl. Phys., **A837**, 26 (2010).
[36] A. Adare *et al.*, Phys. Rev. Lett., **104**, 132301 (2010).
[37] R. A. Lacey *et al.*, Phys. Rev. Lett., **98**, 092301 (2007).
[38] A. Adare *et al.*, Phys. Rev. Lett., **98**, 172301 (2007).
[39] Z. Xu, C. Greiner, and H. Stocker, Phys. Rev. Lett., **101**, 082302 (2008).